Electron Dynamics in Dendrimers

T. Sean Elicker and Deborah G. Evans*

Quantum Chemistry Research Group, Albuquerque High-Performance Computing Center and Department of Chemistry, University of New Mexico, Albuquerque, New Mexico 87131

Received: May 17, 1999; In Final Form: September 2, 1999

Electron transfer dynamics in extensively branched macromolecules (dendrimers) is studied using time-dependent quantum mechanical techniques. A split operator method that fully exploits the Cayley tree topology of these macromolecules is developed within a tight-binding model Hamiltonian. Solvent effects are simulated by time-dependent random fluctuations; this dephasing eliminates the localized oscillations that characterize the nonsolvated dynamics, and results in decay of the electron density from an initially photoexcited state. Electron transfer is asymmetric depending on the site of initial excitation, and solvent fluctuations in general enhance the directed transport within the structure. Some dendrimers, particularly those with a certain extended structures show enhanced transport toward their central nodes. The efficiency of electron transfer to the central node depends on both the dendrimer structure and the characteristics of the solvent fluctuations.

I. Introduction

Dendrimers have been the topic of numerous synthetic studies in the last few years. Sophisticated molecules with a wide range of monomer units ranging from silicon to porphyrins have been assembled with extensively branched tree structures.[1] They are currently the only synthetic realizations of the Cayley tree structure;[2] this novel topology, along with the existence of precise control over the size of the product molecule, makes dendrimers a useful model for investigating the dependence of physical properties on molecular size and topology. Recent experiments examining the physical and spectroscopic properties of certain classes of dendrimers provide preliminary evidence that some dendrimers may have applications in molecular electronics, as LEDs[3] and single-molecule photonic antennae.[4]

A number of theoretical papers have focused on the classical simulation of dendrimer structure.[5] Molecular dynamics simulations of large dendrimers in solvent have successfully explained phenomena like the uptake of small chromophores into a dendrimer structure, for example.[6] Effective coupling matrix elements for electron transfer have been studied by Risser et al.[7] They have shown that the connectivity gives rise to different electronic properties from those of corresponding linear polymers. By focusing on the electron pathways model of electron transfer[8] in macromolecules, Risser et al.[7] were able to show that at certain levels of static disorder in the dendrimer Hamiltonian, there is a growth of strong paths to the dendrimer surface in comparison with their linear counterparts. Interestingly, they have found that static disorder in dendrimers may therefore increase coupling between the donor and acceptor sites.

Recent spectroscopic studies on two classes of dendrimer structures have provided interesting results.[9−11] The structures are phenyl dendrimers, where the branching nodes are 1,3,5-trisubstituted benzene and the node-to-node linkage is via various bridging systems (see for example, ref 9). These macromolecules are generally synthesized by a convergent method,[12] in which each of the three main branches are formed independently. The final step of the synthesis then couples these branches to a central molecule. This method is know to be superior to divergent methods,[13] where the dendrimer is grown outward from an initial core; indeed, convergent synthesis practically guarantees a Cayley tree structure in the product, and the size limitations of that product are due solely to steric interactions between elements of the outermost layer, or "generation". By modifying the synthesis slightly, a selected number of paradisubstituted benzenes (and accompanying bridging groups) may be inserted between successive generations of branching nodes. These structures, called extended Cayley dendrimers, manifest different spectroscopic properties from their compact counterparts. In extended structures, the electronic absorption peak maximum exhibits a red shift with increasing generation number, whereas in compact dendrimers no such shift occurs. This energy gradient could be exploited to create an energy funnel in these structures.[9] The collective electronic oscillator approach[14] for calculating the absorption spectrum has been applied to a series of these phenylacetylene-type dendrimers.[15] It has been shown that the electron-hole pairs that contribute to the elementary collective excitations are well-localized. This has enabled the calculation of the absorption spectra of a series of dendrimers to be approximated from the absorption profiles of the independent constituent oligomers, and these show a red shift commensurate with the experimental data.

Intermolecular electron transfer studies have been conducted on a variety of systems. For example, encapsulated electroactive molecules have been synthesized with iron−sulfur cluster cores.[16] Photoinduced electron transfer rates from metalloporphorin dendrimers to solvated MV^{2+} ions have been recorded spectroscopically[17] and electron transfer from dendrimeric metallophthalocyanines to MV^{2+} has been monitored via fluorescence quenching.[18] Other studies have used electron spin resonance to study electron transfer from carboxylated dendrimers to C_{60} as a function of the number of dendrimer generations.[19] Recently, intermolecular photoinduced experiments have been carried out on a series of phenylacetylene dendrimers with geometries very similar to the phenylacetylene dendrimers studied spectroscopically as photonic antennae.[20] These measurements are a prelude to studies on intramolecular electron transfer with suitable donor and acceptor functionalities.

10.1021/jp991606g CCC: $18.00
Published on Web 11/05/1999

These studies demonstrate that dendrimers can act as suitable bridging media for electron transfer between redox centers, and indicate the feasibility to effect photoinduced electron transfer in dendrimers with a suitable choice of electron/donor functionality at the core and on the periphery.

A study of electron transfer within dendrimers is therefore timely. In particular, this study focuses on the electron dynamics of photoinduced electron transfer in both condensed and extended dendrimeric structures. The role of solvent fluctuations on electron transfer is examined and the behavior compared with linear donor−bridge−acceptor molecules. Unlike the work of Risser et al.,[17] our research focuses on the time evolution of electron population dynamics within the dendrimeric structure. In order to extend this to more sophisticated models in the future, we have developed a split-operator method that exploits the unique dendrimer connectivity, and incorporates time-dependent solvent fluctuations as discussed in Section II. In Section III, the electron transfer dynamics is simulated for several classes of condensed and extended dendrimer structures. The effects of changes in dendrimer size, and particularly geometry, are examined. Changes induced by solvent fluctuations are studied both in terms of the magnitude and time scales of the solvent fluctuations. A discussion of the experimental ramifications of these results is presented in the final section.

II. Methods

We have devised an algorithm for the time evolution of an initial photoexcited state. The algorithm, DEVO (*d*endrimer *evo*lution), is a split operator method and it is specifically designed to perform quantum-dynamic simulations of electron transport in dendrimers. Although DEVO is applicable to both electron and exciton dynamics, this study is concerned exclusively with electron dynamics following photoexcitation. The tight-binding Hamiltonian for electron transport in a dendrimer is written as

$$\hat{\mathbf{H}} = \sum_{ij} \beta_{ij}(a_i^\dagger a_j + a_j^\dagger a_i) + \sum_i \epsilon_i a_i^\dagger a_i + \Phi(t) \qquad (1)$$

where we use the parameter values of Felts et al.:[21] $\epsilon = 1500$ cm^{-1} for the donor and acceptor sites and zero for all other sites; $\beta = 300$ cm^{-1} for nearest neighbors and zero otherwise. Further details on the workings of the DEVO algorithm may be found in Appendix A.

The $\Phi(t)$ term represents the influence of the solvent on the electron process

$$\Phi(t) = \sum_i \phi_i a_i^\dagger a_i + \sum_{ij} \mu_{ij}(a_i^\dagger a_j + a_j^\dagger a_i) \qquad (2)$$

Both the on-site ϕ_i and off-diagonal μ_{ij} components are described as uncorrelated Gaussian noise, and in this model represent a way of incorporating the solvent influences into a calculation of the electron dynamics. Unlike more phenomenological approaches,[23] these effects can be incorporated into the model using further calculations. For example, for electron transfer in a particular dendrimer in a specific solvent, these fluctuating matrix elements can be obtained from simulations of the system. In particular, on-site fluctuations could be determined from ab initio reaction field calculations and off-diagonal coupling matrix elements could be determined by calculating the fluctuating site−site distances using classical molecular dynamics simulations and correlating these with changes in the bond integral.[22] We represented different solvents by changing the magnitude of the fluctuations and/or the characteristic updating time τ_{solv} of the fluctuations. The three different solvation regimes are characterized by the magnitude of the standard deviations of the two types of fluctuations: $\langle \phi_i(t), \phi_i(t') \rangle = \sigma_i \cdot \delta(t - t')$ and $\langle \mu_{ij}(t), \mu_{ij}(t') \rangle = \sigma_{ij} \cdot \delta(t - t')$. We set $\sigma_i = 0.04\epsilon_i$ and $\sigma_{ij} = 0.0001\beta_{ij}$ in the nearly-coherent regime I; $\sigma_i = 0.1\epsilon_i$ and $\sigma_{ij} = 0.01\beta_{ij}$ in regime II; finally, $\sigma_i = 0.25\epsilon_i$ and $\sigma_{ij} = \beta_{ij}$ for the strongly solvated regime III. The organometallic center and radially symmetric arrangement of organic centers is reminiscent of donor/acceptor models in linear conjugated systems, which motivated our choice of energetic parameters from earlier work on such linear systems.[21,23]

In our simulations, we have examined the nature of the evolution of electron density through a series of structurally distinct dendrimers, and the spatial character of the evolving electron density in these structures. Using DEVO to compute the wavefunction at each time step enables the evaluation of electron probability density on each node in the dendrimer, as well as the total density on each generation. In order to investigate possible wavefunction localization, we have calculated the inverse participation ratio.[24,25]

$$P^{-1} = \sum_i (\Psi_i \Psi_i^*)^2$$

In a system with N sites, this ratio is unity for a perfectly localized state, and equal to $1/N$ for a completely delocalized state. Therefore, P (the participation number) gives a rough estimate of the extent of wavefunction delocalization over the dendrimer sites. We also compute the ratios of the site densities to the value $1/N$, to study how the asymptotic probability distribution varies from the perfectly delocalized state.

III. Results and Discussion

In order to focus on the general properties of dendrimers with a certain geometrical structure, our study is confined to a class of synthetically well known phenyl-based dendrimers with an organometallic central node. As shown in Appendix A, there is no loss of generality in modeling these dendrimers as benzene nodes with no bridging groups. Recent experimental work has shown that interesting spectroscopic behavior occurs in dendrimers with extended structures,[9] which is different to the behavior observed for condensed, or self-similar structures. To determine whether dendrimers with these different geometries can display radically different behavior in electron transfer experiments, we studied electron transfer dynamics in both condensed and extended dendrimers. Our simulations include condensed dendrimers with three, four, and five generations, denoted hereafter as 3*N*, 4*N*, and 5*N* and a set of three qualitatively different three-generation extended dendrimers: (14), (33), and (52). Schematics of the six structures are shown in Figure 1. The first number in the ordered pair is the size (in terms of nodes) of the three interstitial groups between the center and first branching nodes, while the second number in the ordered pair is the size of the six interstitial groups between these first branching nodes and the outer nodes in the three-generation dendrimer. These particular extended geometries have been selected because each one involves the addition of exactly 27 interstitial nodes to a three-generation dendrimer. This excludes the possibility that variations in dynamics are due to a change in the total number of nodes in the dendrimer. The electron density following photoexcitation is monitored for 100 fs in these simulations, and the solvent-induced fluctuations are updated (on average) every 15 fs. The final data sets are averaged over an ensemble of solvent fluctuations.

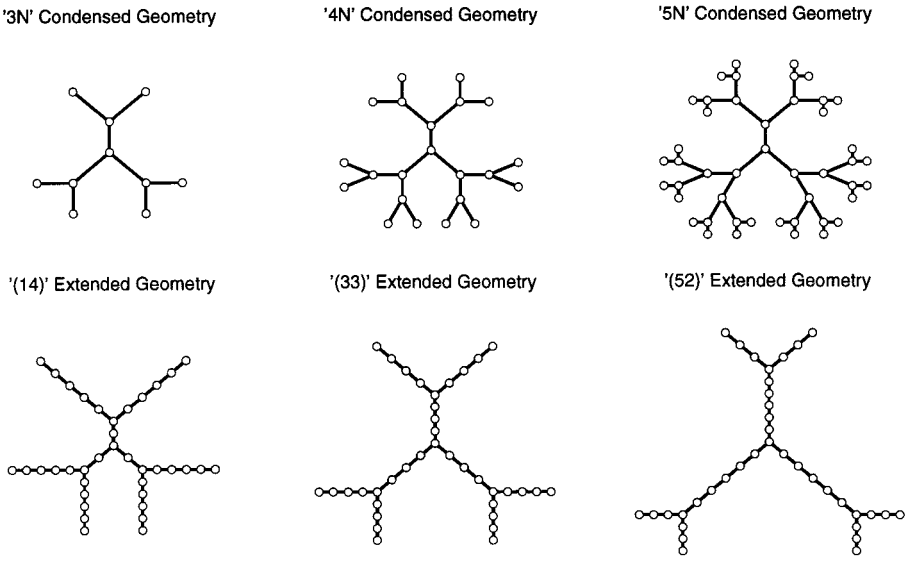

Figure 1. Schematic diagrams of the six dendrimer geometries studied (circles represent chemical units).

Dendrimers in which the outer generation of benzene rings is replaced with a generation of nodes chemically identical to the center node are also studied; such structures are analogous to linear conjugated donor/acceptor systems that have been well-studied elsewhere. Linear systems at high solvent coupling exhibit the phenomenon of bridge trapping, where the measurable electron density is found on the intermediate bridge sites. Figure 2 shows the values of ρ_B/ρ_{B0} for the various dendrimer geometries; ρ_B is the asymptotic total density on all the intermediate (bridge) nodes of the dendrimer, and the zero subscript denotes data from simulations without an outer acceptor layer. Bridge-trapping behavior is observed in those simulations where the electron starts on the center node(SN $=$ 1), but not in those simulations where the electron starts on the outer layer (SN $= N$). In the SN $=$ 1 case, the Cayley tree topology ensures that all paths from the donor (center) to an acceptor are equivalent in length, and the electron transfer system is analogous to linear donor−bridge−acceptor systems. In all solvent regimes, evidence for bridge trapping is found, unlike previous studies on linear systems. This is due to the fact that this model incorporates both on-site and site-site fluctuations which dephase the electron wavefunction on the bridge even at relatively small solvent fluctuations. The SN $= N$ case lacks the symmetry of the SN $=$ 1 case, and electron transfer is different from linear systems if the dephasing time scale is longer than it takes for the electron on one of the periphery sites to move to the center and then be transferred to alternative branches. In fact, the natural bias in the dendrimer geometry for outward movement of quasiparticles in the incoherent (strong solvent coupling) regime has previously been illustrated using simple rate equations.[10] That our results differ for SN $=$ 1 or N tends to support that this is also the situation for typical electron transfer in dendrimeric bridge molecules for a range of solvent regimes where the fluctuations are on the order of 10−15 femtoseconds. Thus, the SN $= N$ system is not analogous to a linear donor-acceptor system, and the dynamics of these systems is asymmetric in terms of where the excitations are initiated. As shown in Figure 2, ρ_B/ρ_{B0} is less than one for the SN $= N$ simulations, which is evidence that less electron density is found on the bridge sites in those simulations with an outer layer of acceptor nodes. This suggests that for the case with no acceptor nodes on the periphery, electron transfer to the center takes place, and then the less efficient back transfer to the outer nodes occurs, creating a buildup of electron density on the bridge sites as the dynamics is dephased by the solvent-induced fluctuations.

There is evidence of substantial localization in all of our simulations. Figure 3 shows the participation number P in dendrimers of various geometries, as compared to the total number of nodes in the dendrimer. In all cases, the number of nodes participating in the wavefunction is much less than the total number of nodes. P increases as the stochastic fluctuations increase, indicating that the destruction of interferences in these finite systems have more impact on localization than the structural distortion induced by the solvent. The degree of localization was much smaller for simulations in which the excitation begins on the outer layer of the dendrimer; this provides further evidence that the spatial anisotropy of such simulations has a real effect on the observed asymmetric dynamics.

Photoinduced electron transfer experiments have recently demonstrated intermolecular electron transfer between phenylacetylene dendrimers and donor molecules in the surrounding solution.[20] The following section is therefore focused on in dendrimers without an outer acceptor layer, and the exploration of the possibility that certain structures may be capable of directed electron transport of the electron density from the outer layers to the center node. To compare the relative abilities of the various structures to do this, $\rho_{tot} = \int_0^{t_f} \rho_c(t) dt$, where the integral is over the entire time interval $[0,t_f]$ of the simulation, is calculated. For SN $= N$ simulations, this integral provides a measure of how effectively the electron density is transferred from the outer layer to the central node, and could be observed as the integrated emission intensity from a fluorescent central core over this time period. Figure 4 shows ρ_{tot} for the six structures in this set of experiments. The efficiency of direct electron density to the central nodes of the condensed structures decreases exponentially with the generation number, but this may be a consequence of the number of nodes between the center and outer layer of the dendrimer. Casting the dependence in terms of this radius r_N allows for a direct comparison of the condensed and extended structures. The lack of relative difference in efficiency between the three extended structures is expected, because their large r_N values (6, 7, and 8) lead to small efficiency differences. This result is supported by examining the effective coupling elements between an outer-layer node and the central node for the three extended structures. As shown

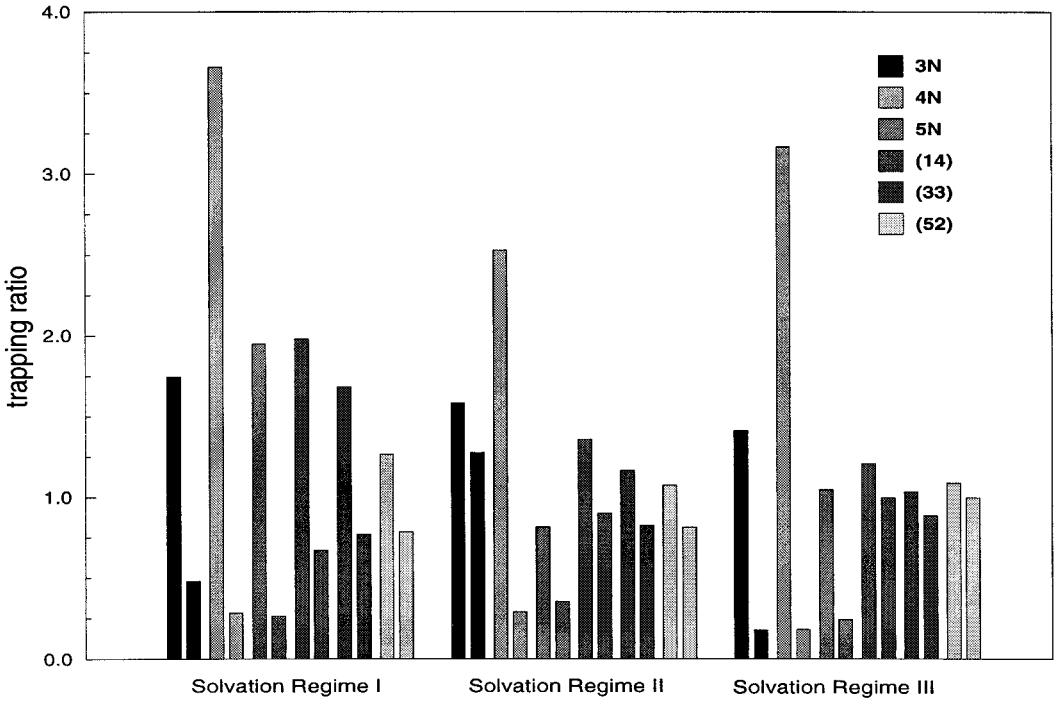

Figure 2. Trapping ratio (ρ/ρ_{B0}) for various dendrimer geometries with SN = 1 (left-hand bar) and SN = N (right-hand bar).

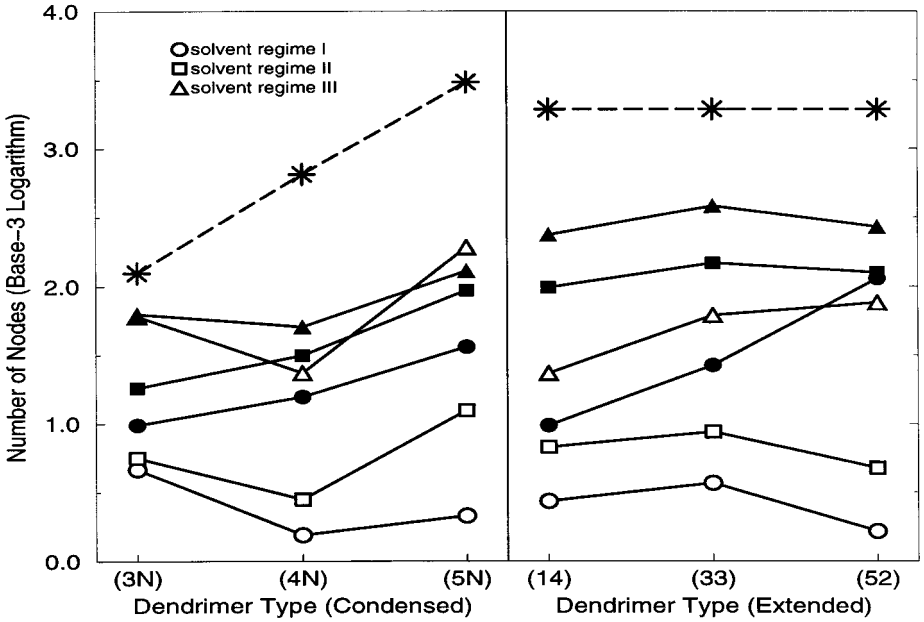

Figure 3. Comparison of participation number for simulations in the three solvent regimes described in Section II. Open symbols denote simulations with STARTNODE = 1, filled symbols denote simulations with STARTNODE = *N*, and asterisks denote the total number of nodes in the dendrimer.

in Appendix B, there is a negligible difference between the three effective couplings for $|\beta|$ values less than one-half of the magnitude of the on-site energies. Nevertheless, the efficiency of the (52) structure is higher than expected , given its increased r_N, in comparison with the condensed geometry. The increased efficiencies of the extended structures must therefore arise from other considerations.

The electron densities on each dendrimer node vary in an oscillatory manner in the absence of solvent; although explicit oscillations are not apparent in the stronger solvent regimes, the timescales of the unsolvated recurrences will affect the observed electron dynamics in the solvated system. Figure 5 shows the total generation densities for four three-generation structures in an unsolvated dendrimer. The behavior for the three extended structures is qualitatively similar, but the timescales for various components of the dynamics vary. For example, Figure 6 graphs the timescales for two components: (i) the first minimum of the density of the initial node, and (ii) the first maximum in the density of the branching node nearest to the initial node for four similar dendrimers. The relationship between structure and time scales is easily seen: decay out of the initial node is independent of the dendrimer size, while the growth on the first branching node depends on the number of monomer spacers in a regular fashion.

The results shown in Figure 4 are obtained by updating the solvent fluctuations every 15 fs (realistic for a generic polar solvent). Different solvents will have different relaxation times, and the variation of dendrimer timescales shown above indicates

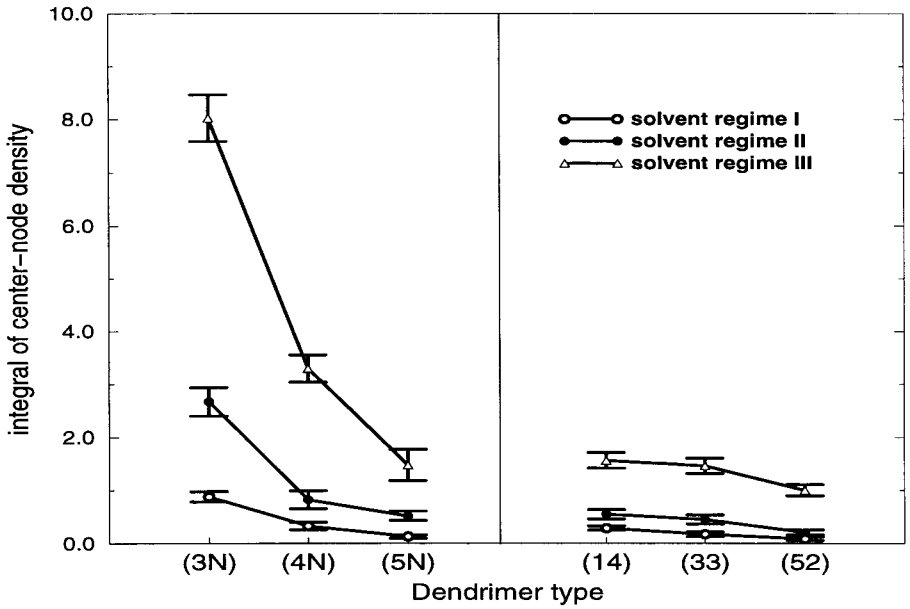

Figure 4. Comparison of ρ_{tot} values for six dendrimers, in the three solvent regimes described in Section II.

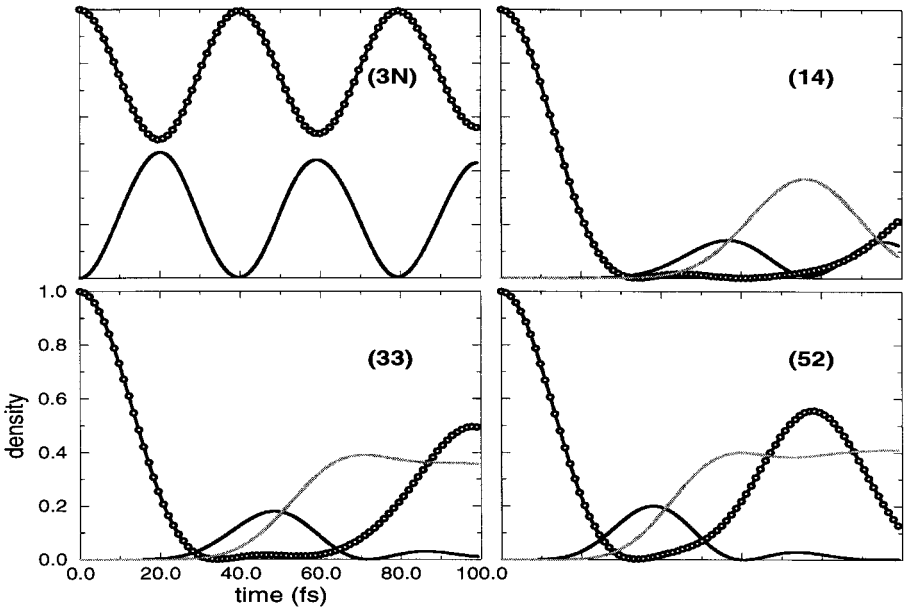

Figure 5. Unsolvated dynamics of (3*N*), (14), (33), and (52), showing the total density on the initial node (circles), the inner branching nodes (solid), and the inner group of interstitial nodes (gray).

that the dynamics is closely linked to the statistics of the solvent. Figures 7 and 8 show ρ_{tot} for the dendrimer families (5*m*) ($1 \leq m \leq 4$) and (*m*2) ($1 \epsilon m \leq 5$). For each structure, ρ_{tot} was calculated in four different solvents, with equivalent fluctuation magnitudes but different timescales. The update times for the fluctuations of the four solvents are $\tau_{solv} = 7$, 15, 30, and 60 fs respectively. For a fixed value of τ_{solv}, the efficiency tends to decrease as r_N increases. The increasing radius increases the recurrence timescales for densities of the inner nodes, so that solvent relaxation results in less electron density trapped near the center of the dendrimer in structures with larger r_N. In such structures, density moves to the center via repeated trapping, and the overall efficiency is lower. This effect vanishes as τ_{solv} increases, for two reasons: the longer solvent timescale allows for significant trapping in the inner regions even for those structures with longer recurrences timescales; also, there are far fewer relaxation steps in the simulation for large τ_{solv}, so structural differences are less important.

The r_N dependence is important; in the 15 fs solvent, the efficiency of the three-generation condensed structure is many times greater than any of the (5*m*) structures, and more than twice as great as the most efficient structures in the (*m*2) family. This may not translate into a preference for condensed structures in devices, however; we expect that molecular volume will also be an important characteristic for directed transfer applications, and (for example) (52) has 4 times as many benzene nodes as (3*N*).

Along with the strong dependence of efficiency on r_N, the relative sizes of the two interstitial groups are also important. For example, the data for (*n*2) shows that, in all four solvents, the drop off in efficiency between (22) and (32) is less than the drop off between (32) and (42). In three-generation structures where r_N does not change by more than one, those dendrimers with more interstitial nodes in the innermost group were more efficient at funneling electron density to the center. Table 1 shows comparison of (22) with various structures having the

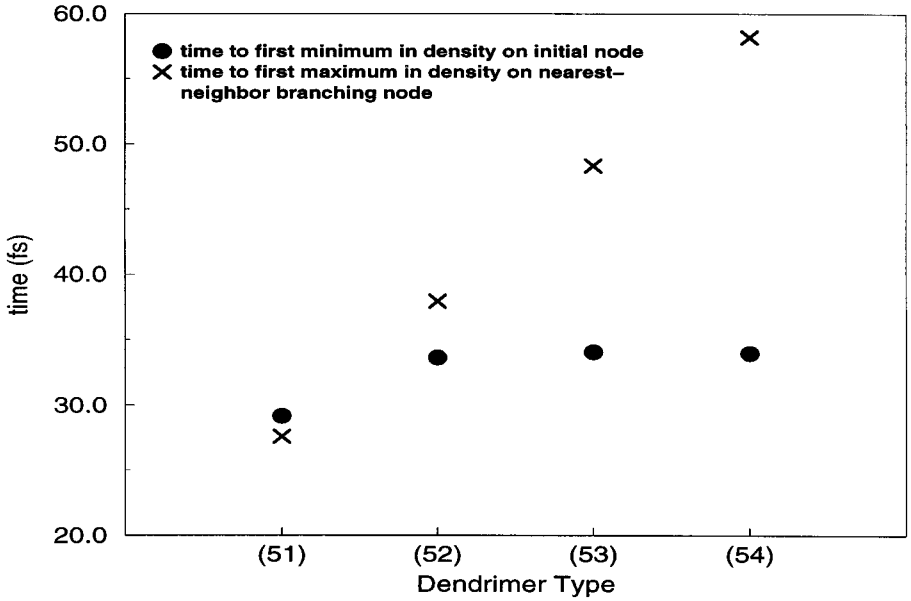

Figure 6. Comparison of two particular timescales for the (5*n*) family of extended dendrimers, $n = 1, 2, 3, 4$.

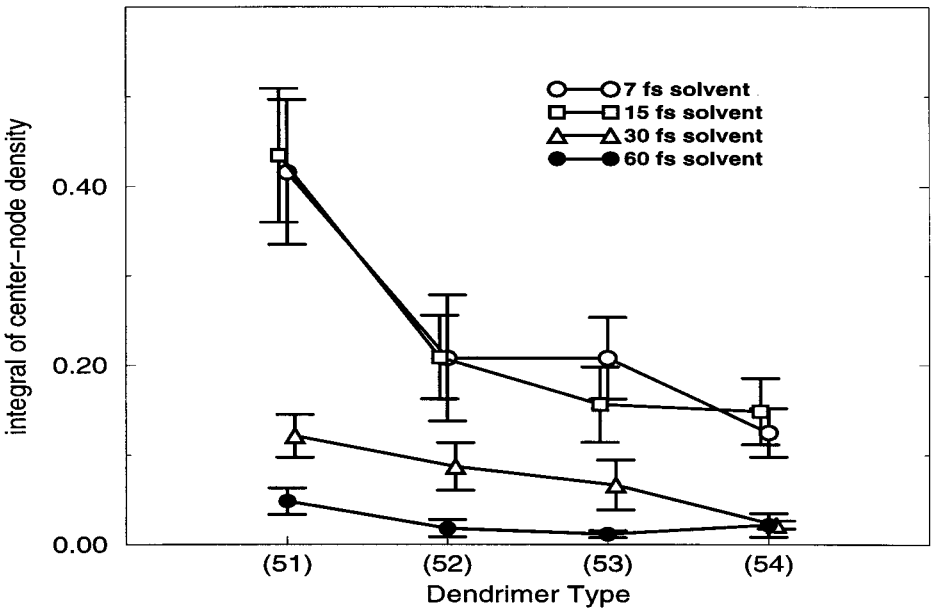

Figure 7. ρ_{tot} values for the (5*n*) family of extended dendrimers, $n = 1, 2, 3, 4$.

same r_N value. The efficiencies of (13) and (22) are comparable, while (31) is nearly 150% more efficient. The trend does not continue, however; (40) is only about 60% as efficient as (22); the complete absence of one interstitial group changes the underlying topology in addition to altering the recurrence time scales.

This importance of the relative sizes of the interstitial groups can also be seen in four-generation dendrimers. In Table 2, three structures that (as above) have the same r_N value are compared in a 15 fs solvent.

The (321) structure is more than twice as efficient as either the (420) or the (402) structures, which is consistent with our hypothesis that structures like $(n_1, n_2, ..., n_K)$ with $n_i > n_i + 1$ are the most efficient among those with the same r_N value. Note that, to a lesser extent, (420) is more efficient than (402), although the presence of the null interstitial groups complicates a direct comparison. Indeed, the efficiency of (302) is less than that of (321), despite the fact that the latter structure has a larger radius.

IV. Conclusions

This study examines the electron transfer dynamics in various dendrimer structures and the effects solvent fluctuations have on those dynamics. To perform these calculations on large dendrimers at the atomistic scale and include time-dependent solvent fluctuations, we have developed a split-operator algorithm (DEVO) to study electron dynamics in dendrimers. This algorithm exploits the Cayley tree structure of dendrimers and is consistently about 40% faster than the checkerboard algorithm. However, DEVO is particularly well-suited to parallelization, and simple scaling arguments increase its efficiency over the checkerboard algorithm to several orders of magnitude for reasonable-sized dendrimers of 7−8 generations.

Intermolecular electron transfer in analogs of phenylacetylene dendrimers has recently been observed,[20] and given a suitable choice of donor and acceptor sites, it appears that intramolecular electron transfer in dendrimers will soon be effected. Experimental[9] and theoretical[15] work on the spectroscopic behavior

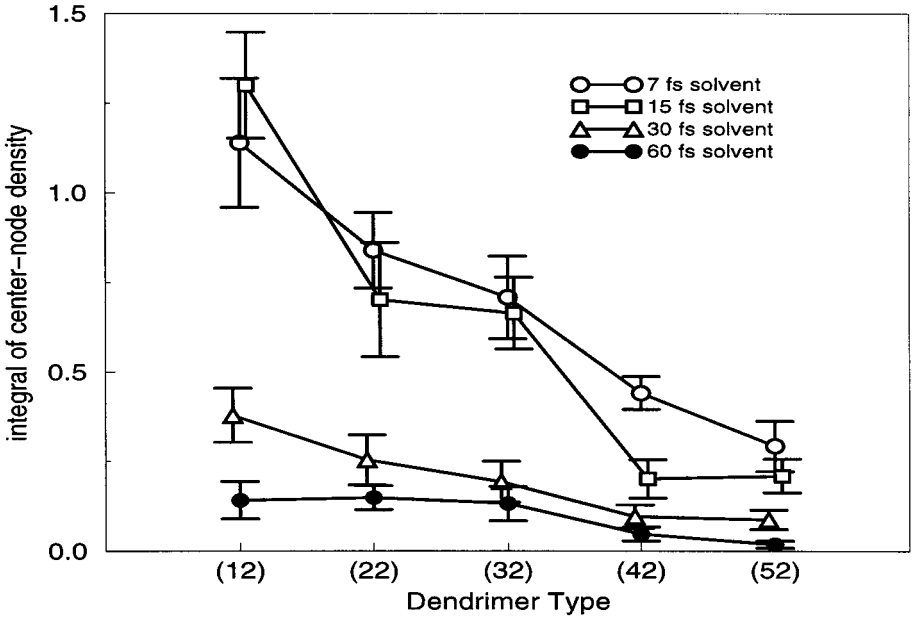

Figure 8. ρ_{tot} values for the (*n*2) family of extended dendrimers, $n = 1, 2, 3, 4, 5$.

TABLE 1: Efficiencies for a Family of Dendrimers with $r_N = 5$, in a 15 fs Solvent

structure	r_N	$\rho_{tot}(\tau_{solv} = 15$ fs)
(22)	5	0.7010 ± 0.15916
(13)	5	0.7939 ± 0.09751
(31)	5	1.0353 ± 0.14736
(40)	5	0.4849 ± 0.08159

TABLE 2: Values of ρ_{tot} for a Group of Four-Generation Extended Dendrimers

structure	radius	$\rho_{tot}(\tau_{solv} = 15\ fs)$
(420)	8	0.1243 ± 0.03259
(402)	8	0.1024 ± 0.03446
(321)	8	0.2525 ± 0.04472
(302)	7	0.2284 ± 0.04849

of phenylacetylene dendrimers has shown that for dendrimers of a particular extended geometry, energy funneling can occur. It has been demonstrated that the spectroscopic behavior of these extended dendrimers is quite different from those with condensed geometries. In this study we have focused on determining whether these two types of dendrimer structure show different electron transfer behavior as well. In particular, we have examined a number of geometries in order to determine if the extended structures are more efficient in transferring an electron from the periphery to the center in a photoinduced electron transfer process.

We have studied electron transfer in dendrimers with organometallic donor sites at the core, both with and without electroactive groups on the periphery. All these structures have trisubstituted benzene molecules as the regular nodes of the dendrimer branches. Our study focuses on the behavior of four related families of geometric arrangements: the first set of simulations were performed on condensed dendrimers with three, four, and five generations, as well as three different extended geometries that have disubstituted nodes between successive generations of branching nodes. All our simulations included solvent effects through stochastic fluctuations of the Hamiltonian matrix elements; the magnitudes of these effects—along with the values of the matrix elements—were taken from previous studies on electron transfer in donor-acceptor linear conjugated systems.[21,23]

When a layer of trapping acceptor nodes was placed at the outer edge of these dendrimers, we found analogies between the resulting dynamics and the dynamics of the linear donor-acceptor systems. In particular, we found evidence of bridge trapping, where significant electron density is found on the nodes between the center and the outer acceptor layer in simulations where the electron density was initially on the central node. If the electron density was initially located on one of the outer nodes, no bridge-trapping occurs as the electron transfer to the center and subsequent branches is now inherently asymmetric, and unlike the linear donor−acceptor bridge systems.

Our studies indicate that strong solvent fluctuations may increase the efficiency of electron transfer to the central core, and that the different types of extended dendrimers do indeed display different behavior for electron transport to the central node in simulations where the electron density was initially at the periphery. We found that, in general, the efficiency of both condensed and extended dendrimers decreases as the radius (number of nodes between the outer node and the center) increases, but the efficiency of extended structures is larger than that of a condensed dendrimer with the same radius. Our data on nonsolvated dynamics shows a strong correlation between the size of interstitial groups and the timescales of electron density recurrences for the various generations in the dendrimer. In many of the structures we studied, the relationship between these recurrence timescales and the relaxation time of the solvent can be directly linked to the directed electron transport to the dendrimer core. There are also specific structural considerations: for example, the decrease in efficiency from (22) to (32) is smaller than between other pairs of successive structures in the (*n*2) family, and among dendrimers of equal radius those with interstitial groups that decrease with distance from the center tend to have higher efficiency of transport to the center.

Attempts to increase the sophistication of describing the solvation effects on the electron transfer are currently underway. Using the DEVO algorithm with solvent fluctuation data extracted from classical molecular dynamics simulations, specific experimental systems (e.g., Fe-S cluster dendrimers[16]) can be described realistically. These results can then be compared with phenomenological approaches[23] and the dissipative

Redfield models of long range electron transfer used by Friesner et al.[21]

Acknowledgment. The authors would like to thank the National Science Foundation (NSF-CAREER), the donors of the Petroleum Research Fund administered by the American Chemical Society, and The Albuquerque High-Performance Computing Center for their support of this research, and Mark Mothersbaugh and his group for their contribution.

Appendix A

The DEVO algorithm decomposes the Hamiltonian (eq 1) in a way that facilitates construction of the propagator for the associated time-dependent Schrödinger equation. DEVO is a simple extension of the checkerboard algorithm,[24,26] where the Hamiltonian is shredded into pairs of interactions and the full propagator $\hat{\mathbf{A}} = \exp[-i\hat{\mathbf{H}}(t)\cdot\delta t]$ is evaluated using split operator techniques. As in other studies,[7,28] this algorithm specifically exploits the topology of the dendrimer. However, DEVO is a split-operator method that replaces the full short-time propagator with an product of simpler propagators that update the evolution of those wavevector coefficients corresponding to a particular subset of nodes. DEVO decomposes the overall propagator $\hat{\mathbf{A}}$ into $\hat{\mathbf{A}}_0\cdot\Pi_i\hat{\mathbf{B}}_i$. The operator $\hat{\mathbf{A}}_0 = \exp[-i\hat{\mathbf{H}}_0(t)\cdot\delta t]$ describes the evolution of the central node and the three benzene nodes adjacent to those connector sites. The sub-Hamiltonian matrix for constructing this evolution operator is

$$\hat{\mathbf{H}}_0 = \begin{vmatrix} \epsilon_0 & \beta_0 & \beta_0 & \beta_0 \\ \beta_0 & \epsilon_1 & 0 & 0 \\ \beta_0 & 0 & \epsilon_1 & 0 \\ \beta_0 & 0 & 0 & \epsilon_1 \end{vmatrix}$$

where ϵ_0 is the on-site energy of the central node, ϵ_1 is the on-site energy of the neighboring benzene nodes, and β_0 is the overlap between the central node and its neighbors. Similarly, the $\hat{\mathbf{B}}_i$ describe the evolution for each branching node and the two adjacent benzene nodes in the next generation outward. These three-node evolution operators are constructed from sub-Hamiltonian matrices similar to the above matrix

$$\hat{\mathbf{H}}_0 = \begin{vmatrix} 0 & \beta & \beta \\ \beta & \epsilon_1 & 0 \\ \beta & 0 & \epsilon_1 \end{vmatrix}$$

with β the overlap between two benzene nodes. Note that the (1,1) entry of $\hat{\mathbf{H}}_i$ is set to zero, to avoid double-counting; that matrix element is already accounted for in either the (2,2) or the (3,3) entry of the submatrix from the next generation inward. Operating on the full-system wavevector with this outward cascade of evolution operators is thus an approximation of the total propagator for the system. Figure 9 is a schematic of how this cascade is performed in a three-generation dendrimer. In a typical dendrimer, the problem of diagonalizing a $(3\cdot2^{N-1} - 2) \times (3\cdot2^{N-1} - 2)$ matrix is replaced by the diagonalization of a single 4×4 matrix and $3\cdot(2^{N-2} - 1)3 \times 3$ matrices.

Many dendrimers have connectors (e.g., oxygen centers and acetylene groups) between adjacent nodes, but DEVO is easily adapted to such systems. In our formalism, such a bridging group is treated as a single interstitial node, so that the sub-Hamiltonian matrices for the bridged dendrimer are

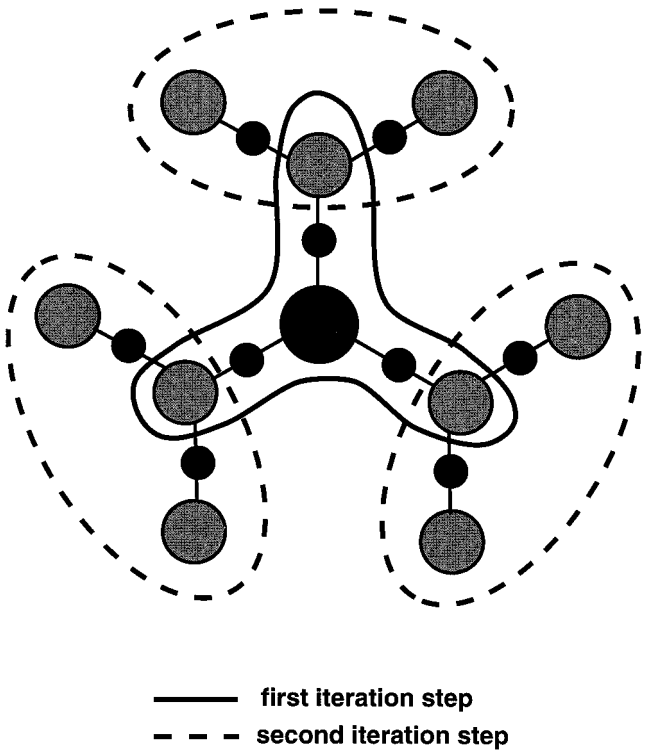

Figure 9. Decomposition scheme for a three-generation dendrimer with connector nodes.

$$\hat{\mathbf{H}}_0 = \begin{vmatrix} \epsilon_0 & \beta_0 & \beta_0 & \beta_0 & 0 & 0 & 0 \\ \beta_0 & \epsilon_2 & 0 & 0 & \beta_1 & 0 & 0 \\ \beta_0 & 0 & \epsilon_2 & 0 & 0 & \beta_1 & 0 \\ \beta_0 & 0 & 0 & \epsilon_2 & 0 & 0 & \beta_1 \\ 0 & \beta_1 & 0 & 0 & \epsilon_1 & 0 & 0 \\ 0 & 0 & \beta_1 & 0 & 0 & \epsilon_1 & 0 \\ 0 & 0 & 0 & \beta_1 & 0 & 0 & \epsilon_1 \end{vmatrix}$$

and

$$\hat{\mathbf{H}}_i = \begin{vmatrix} 0 & \beta_1 & \beta_1 & 0 & 0 \\ \beta_1 & \epsilon_2 & 0 & \beta_1 & 0 \\ \beta_1 & 0 & \epsilon_2 & 0 & \beta_1 \\ 0 & \beta_1 & 0 & \epsilon_1 & 0 \\ 0 & 0 & \beta_1 & 0 & \epsilon_1 \end{vmatrix}$$

where the on-site energies of the central, benzene, and bridging nodes are given (respectively) by ϵ_0, ϵ_1, and ϵ_2; the central−bridging and bridging−benzene overlaps are given by β_0 and β_1. These two matrices may now be reduced to 4×4 and 3×3 matrices via Löwdin decomposition;[27] the reduced matrices will have the same form as the matrices in the DEVO algorithm, with the non-zero entries now algebraic combinations of the various elements of the original matrices. The DEVO algorithm only requires that the two matrices have the form shown above, so it works perfectly well with the reduced matrices of the bridged dendrimer.

DEVO is also applicable for extended dendrimers, which have a number of disubstituted benzene nodes between branching benzene nodes of successive generations. We chose to include these disubstituted nodes directly in the algorithm (rather than calculating effective matrix elements as above) because the electron population of these new nodes was of interest to us. Each set of interstitial nodes introduces a tridiagonal matrix into the decomposition of the Hamiltonian, since these new nodes−

along with the branching nodes at each end--form a linear chain. These tridiagonal matrices are used to construct sub-propagators which are inserted at the proper place in the DEVO evolution cascade.

The development of a time-evolution algorithm like DEVO is motivated by the fact that the Hamiltonian is explicitly time-dependent as a result of the solvent induced fluctuations; the use of many small matrices speeds up the diagonalization process, allowing several updates without making the simulation run-time prohibitively long. This formalism also works well in simulations where, due to steric or other factors, the effect of the solvent is spatially anisotropic.

Appendix B

For the three different three-generation extended structures—(14), (33), and (52)—explicit algebraic formulae for the effective coupling elements (ECE) between the central node and a node in the outer generation can be calculated. This is done via the Lowdin decomposition;[27] in each case the Hamiltonian matrix representing an entire branch of the dendrimer is reduced to a 4×4 matrix for the central node, the single branching node, and the two nodes on the outer layer. (For details on these structures, see Figure 1.) In the following formulae, the on-site energy of benzene nodes is denoted by a; the energy scale is assumed to be shifted such that the on-site energy of the donor−acceptor nodes is zero. The benzene−benzene overlap is given by b, and B is the overlap between a benzene node and a donor−acceptor node (although the outer layer of nodes in most of our simulations were benzenes, we included the more general case in these calculations for completeness.). For clarity, D_n denotes the determinant of an $n \times n$ tridiagonal matrix with a on the main diagonal and b on both subdiagonals.

The three ECE are

$$\mathbf{(14)} = \frac{\left(\frac{B^2 D_3}{D_4}\right)\left(\frac{Bb}{a}\right)\left(\frac{Bb^4}{D_4}\right)}{\left[a - \frac{b^2}{a} - \frac{2b^2 D_3}{D_4}\right]\left(\frac{B^2 D_3}{D_4}\right) + \left(\frac{Bb^4}{D_4}\right)^2}$$

$$\mathbf{(33)} = \frac{\left(\frac{B^2 D_2}{D_3}\right)\left(\frac{Bb^3}{D_3}\right)^2}{\left[\frac{3bD_2}{D_3} - a\right]\left(\frac{B^2 D_2}{D_3}\right) - \left(\frac{Bb^3}{D_3}\right)^2}$$

$$\mathbf{(52)} = \frac{\left(\frac{aB^2 b^3}{D_5}\right)\left(\frac{Bb^2}{D_2}\right)^2}{\left[\frac{2ab^2}{D_2} + \frac{b^2 D_4}{D_5} - a\right]\left(\frac{aB^2}{D_2}\right) - \left(\frac{Bb^2}{D_2}\right)^2}$$

For the relative energies used in our simulations (the magnitude of the overlap matrix elements never more than 25% of the on-site energy) the difference between these three ECE is negligible. There are quantitative changes if the outer layers are taken to be benzene rings rather than acceptor nodes, but the difference between the ECE for these three structures are still essentially equal in magnitude.

References and Notes

(1) (a) Wooley, K. L.; Hawker, C. J.; Pochan, J. M.; Frechet, J. M. J. *Macromolecules* **1993**, *26*, 1515; (b) Tomalia, D. A.; Naylor, A. M.; Goddard, W. A. III. *Angew. Chem. Int. Ed. Engl*. **1990**, *29*, 138; (c) Tomalia, D. A.; Durst, H. D. *Top. Curr. Chem.* **1993**, *165*, 192; (d) Mansfield, M. L. *Polymer* **1827**, *35*, 1827.

(2) Ziman, J. M. *Models of Disorder*; Cambridge University Press, Cambridge, U.K., 1979.

(3) Moore, J. S.; Wang, P.; Liu, Y.; Devadoss, C.; Bharathi, P. *Adv. Mater*. **1996**, *8*, 237.

(4) (a) Barhaim, A.; Klafter, J.; Kopelman, R. *J. Am. Chem. Soc*. **1997**, *119*, 6197; (b) Barhaim, A.; Klafter, J. *J. Phys. Chem. B* **1998**, *102*, 1662; (c) Barhaim, A.; Klafter, J. *J. of Lumin.* **1998**, *76*, 197.

(5) (a) Murat, M.; Grest, G. S. *Macromolecules*, **1996**, *29*, 1278; (b) Mansfield, M. L.; Klushin, L. I. *Macromolecules* **1993**, *26*, 4262.

(6) Miklis, P.; Cagin, T.; Goddard, W. A. *J. Am.Chem. Soc.* **1997**, *119*, 7458.

(7) Risser, S. M.; Beratan, D. N.; Onuchic, J. N. *J. Phys. Chem.* **1993**, *97*, 4523.

(8) Skourtis, S. S.; Onuchic, J. N.; Beratan, D. N. *Inorg. Chim. Acta*. **1996**, *243*, 167.

(9) (a) Shortreed, M. R.; Swallen, S. F.; Shi, Z. Y.; Tan, W. H.; Xu, Z. F.; Devadoss, C.; Moore, J. S.; Kopelman, R. *J. Phys. Chem. B* **1997**, *101*, 6318; (b) Shortreed, M. R.; Shi, Z. Y.; Kopelman, R. *Mol. Crys. and Liq. Crys. Sci. Tech. A*, **1996**, *283*, 95.

(10) Barhaim, A.; Klafter, J. *J. Chem. Phys.* **1998**, *109*, 5187.

(11) Kopelman, R.; Shortreed, M.; Shi, Z. Y.; Tan, W. H.; Xu, Z. F.; Moore, J. S.; Barhaim, A.; Klafter, J. *Phys. Rev. Lett*. **1997**, *78*, 1239.

(12) For example: (a) Tomalia, D. A.; Baker, H.; Dewald, J. R.; Hall, M.; Kallos, G.; Martin, S.; Roeck, J.; Ryder, J.; Smith, P. *Polym. J.* **1985**, *17*, 117; (b) Jayaraman, M.; Frechet, J. M. J. *J. Am. Chem. Soc*. **1998**, *120*, 12996.

(13) For example: (a) Hawker, C. J.; Wooley, K. L.; Frechet, J. M.; *J. Chem. Soc., Perkin Trans.* **1993**, *12*, 1287. (b) Huck, W. T. S.; Prins, L. J.; Fokkens, R. H.; Nibbering, N. M. M.; Vanveggel, F. C. J. M.; Reinhoudt, D. N. *J. Am. Chem. Soc*. **1998**, *120*, 6240.

(14) (a) Mukamel, S.; Tretiak, S.; Wagersreiter, T.; Chernyak, V. *Science* **1997**, *277*, 781. (b) Chernyak, V.; Mukamel, S. *J. Chem. Phys*. **1996**, *104*, 444. (c) Tretiak, S.; Chernyak, V.; Mukamel, S. *J. Chem. Phys*. **1996**, *105*, 8914.

(15) Tretiak, S.; Chernyak, V.; Mukamel, S. *J. Phys. Chem. B* **1998**, *102*, 3310.

(16) (a) Gorman, C. B. *Adv. Mater*. **1997**, *9*, 1117. (b) Gorman, C. B.; Parkhurst, B. L.; Su, W. Y.; Chen, K-Y *J. Am. Chem. Soc.* **1997**, *119*, 1141.

(17) Sadamoto, R.; Tomioka, N.; Aida, T. *J. Am. Chem. Soc*. **1996**, *118*, 3978.

(18) Kimura, M.; Nakada, K.; Yamaguchi, Y.; Hanabusa, K.; Shirai, H.; Kobayashi, N. *Chem. Comm.* **1997**, *13*, 1215.

(19) Janssen, R. A.; Jansen, J.; van Haare, J. A. E. H.; Meijer, E. W. *Adv. Mater.* **1996**, *8*, 494.

(20) Devadoss, C.; Bharathi, P.; Moore, J. S. *Macromolecules* **1998**, *31*, 8091.

(21) (a) Felts, A. K.; Pollard, W. T.; Friesner, R. A. *J. Phys. Chem*. **1995**, *99*, 2929. (b) Pollard, W. T.; Friesner, R. A. *J. Chem. Phys.* **1994**, *100*, 5054.

(22) Yates, K. *Huckel Molecular Orbital Theory*; Academic Press, New York, 1978.

(23) Davis, W. B.; Wasielewski, M. R.; Ratner, M. A.; Mujica, V.; Nitzan, A. *J. Phys. Chem. A* **1997**, *101*, 6158.

(24) (a) Evensky, D. A.; Scalettar, R. T.; Wolynes, P. G. *J. Phys. Chem. B* **1990**, *94*, 1149. (b) Evensky, D. A.; Wolynes, P. G. *Chem. Phys. Lett*. **1993**, *209*, 185.

(25) Economou, E. N. *Green's Functions in Quantum Physics*; Springer: New York, 1994.

(26) (a) Hill, N. A.; Whaley, K. B. *Chem. Phys*. **1996**, *210*, 117; (b) Hill, N. A.; Whaley, B. *J. Chem. Phys*. **1993**, *99*, 3707.

(27) Löwdin, P. O. *J. Mol. Spectrosc.* **1963**, *10*, 12; *J. Math. Phys*. **1962**, *3*, 969.

(28) Poliakov, E. Y.; Chernyak, V.; Tretiak, S.; Mukamel, S. *J. Chem. Phys*. **1999**, *110*, 8161.